Vant-Hull, Brian; Karimi, Maryam; Sossa, Awolou; Wisanto, Jade; Nazari, Rouzbeh; Khanbilvardi,
Reza

FINE STRUCTURE IN MANHATTAN'S DAYTIME URBAN HEAT ISLAND: A NEW DATASET

FINE STRUCTURE IN MANHATTAN'S DAYTIME URBAN HEAT ISLAND: A NEW DATASET

Brian Vant-Hull[1], Maryam Karimi[1], Awolou Sossa[2], Jade Wisanto[1], Rouzbeh Nazari[1], Reza Khanbilvardi[1,3]

[1]NOAA-CREST Institute, City University of New York, United States
[2]New York City College of Technology, United States
[3]Department of Civil Engineering, City College of New York, United States

Abstract: A street-level temperature and humidity dataset with high resolution spatial and temporal components has been created for the island of Manhattan, suitable for use by the urban health and modelling communities. It consists of a set of pedestrian measurements over the course of two summers converted into anomaly maps, and a set of ten light-post mounted installations measuring temperature, relative humidity, and illumination at three minute intervals over three months. The quality control and data reduction used to produce the anomaly maps is described, and the relationships between spatial and temporal variability are investigated. The data sets are available for download via the project website.

Correspondence to: Brian Vant-Hull, Tel.: +01 917 318 448; Fax: +01 212 650 8097.
E-mail: brianvh@ce.ccny.cuny.edu

INTRODUCTION

Nearly all studies of the urban heat island have focused on the increase of urban over rural temperatures, a difference which peaks at night due primarily to higher heat storage and nocturnal release; and to radiative trapping in urban canyons (Oke, 1982; Grimmond & Oke, 1999). And yet city inhabitants are understandably more concerned with urban daytime temperatures, even if only slightly higher than daytime rural temperatures (Fast *et al.*, 2005; Gedzelman, 2003; Gaffin *et al.*, 2008). The nocturnal heat island prolongs the health risks of a heat wave, but the intensity is gauged by peak daytime temperatures. Above a certain threshold that varies by city, the heat related mortality rate increases quasi-exponentially with temperature, so that during heat waves the mortality rate becomes very sensitive to changes of a few degrees (Kinney *et al.*, 2008a,b). Variations in building structure, vegetation and albedo within the urban 'archipelago' can result in local temperature differences of several degrees (Yamashita, 1996; Weng *et al.*, 2003, 2008; Stewart *et al.*, 2003; Rosensweig *et al.*, 2006; Pena, 2009; Montavez *et al.*, 2000; Grimmond, 2007; Gaffin *et al.*, 2008; Eliasson, 1996a,b; Comrie, 2000; Bottyan & Unger, 2003). The data set described in this paper is a first step towards creating high resolution (~10^2 m) neighborhood-scale temperature anomaly maps of a highly urbanized area that may benefit the health community while serving as a test bed for physical modelers.

The influence of the urban environment on localized temperature at the neighborhood scale is well understood theoretically (Oke, 1981; Cleugh & Grimmond, 2001; Grimmond 1999, 2007). Urban systems can be modelled physically at the scale of individual buildings (meter scale) where all boundary values can be measured directly, or at the km scale where averaged properties have been inferred from large scale atmospheric response and parameterized as part of numerical weather model packages (Rozensweig *et al.*, 2006; Meir *et al.*, 2013). But due to the complexity of intermediate scales and the inability to directly measure all heat transport and storage parameters, modelers at the multi-building (or neighborhood) scale must resort to case-by-case statistical parameterization based on case study temperature measurements which are typically sparse compared to the scale of neighborhood variability (Bottyán & Unger, 2003; Eliasson, 1996a; Pena, 2009; Weng *et al.*, 2008). The situation is even more complex for daytime versus night time; in addition to heat transport, storage and thermal radiation effects, daytime temperatures are modulated by the shade of buildings and vegetation, and by evaporative cooling that is enhanced by vegetation but inhibited by impervious surfaces (Weng & Schubring, 2003; Steenveld *et al.*, 2011; Rosenzweig *et al.*, 2006; Pena, 2009).

There are three basic approaches to gathering high resolution climate data for urban environments. The first is to employ fixed stations that for logistical and financial reasons may be widely spaced but can collect data over an extended period of time (Comrie, 2000; Fast *et al.*, 2005; Gedzelman, 2003; Meir *et al.*, 2013; Haeger-Eugensson & Holmer, 1999; Montavez, 2000; Preston-White, 1970; Steeneveld *et al.*, 2011). This approach has the advantage of sampling not only over the diurnal cycle but also over a wide range of weather conditions, allowing for adjustments due to the smoothing effects of wind or clouds (Eliasson, 1996a; Montavez *et al.*, 2000; Oke, 1982) or regional circulations caused by urbanization (Gedzelman, 2003; Meir *et al.*, 2013; Heuger-Eugensson & Holmer, 1999), though caution must be used with regard to non-standardized siting of hobby stations (Grimmond, 2010). The second approach is the use of mobile stations deployed across large spatial tracts during a short period of time (Bottyán & Unger, 2003; Comrie, 2000; Eliasson, 1996b; Gaffin *et al.*, 2008; Montavez *et al.*, 2000; Yamashita, 1996). This has the advantage of high resolution in space, but is too intermittent to capture a full statistical set of weather conditions, and requires a substantial commitment to gather data on a regular basis.

The third approach to collecting climate data is via satellite, most notably high resolution thermal-IR capable satellites such as LandSat and ASTER (Pena, 2009; Rosenzweig *et al.*, 2006; Weng & Schubring, 2003; Weng *et al.*, 2008; Weng, 2009). The main advantage of satellite data is the ease of collection. But like mobile measurements, satellite datasets also suffer from the intermittent nature of overpasses under clear conditions that make them unsuitable for most weather analysis. Moreover, surface temperatures retrieved by satellite should not be confused with air temperatures measured by most probes; the surface typically interacts more strongly with the radiative environment and largely serves as an intermediary between radiation and the air near the surface, often creating steep vertical air temperature gradients (Clough & Grimmond, 2008; Eliasson, 1996b; Grimmond & Oke, 1999; Oke 1982; Gaffin, 2013). Satellite observation of highly built up areas such as Manhattan also sample a mix of rooftop and street level surface temperatures, which for high buildings can introduce significant deviations from the surface level.

With these strengths and weaknesses in mind, the dataset presented in this paper consists of a mix of well characterized fixed and mobile measurements at street level. The island of Manhattan in New York City is of interest both as an exemplar of the urban environment, and for its high population density of nearly 27

thousand per km^2. It features a range of elevations, building heights, and street widths (with and without trees); and parkland, commercial and residential sectors of apartments or row houses. The measurements consist of pedestrian mounted temperature and relative humidity surveys in simultaneous parallel transects near the hottest part of the day during the course of two summers, and a set of light-post mounted instruments collecting data continuously during the summer of 2013. The data has been processed for instrument bias and temporal trends and is freely available for download at http://glasslab.engr.ccny.cuny.edu/u/brianvh/UHI. For ease of future study the field campaign data is co-located with data from the US Geological Survey (USGS), the National Building Statistics Database (NBSD), and retrievals of surface properties from the MODIS and LandSat satellites. This data set serves as a complement to the ongoing but coarser resolution NYC MetNet collection of government and hobby weather station data plus wind profilers and radiometric instruments curated at http://nycmetnet.ccny.cuny.edu.

The remainder of this paper describes data collection and processing, with a discussion of data quality and the unique attributes of a data set of this kind. An important part of the data processing is an averaging procedure based on the position of each measurement within each day's statistical distribution rather than the explicit value, which the authors feel is a more robust approach to calculating anomalies. An outline is included of future plans to use this data for short term and climatic forecasts.

DATA COLLECTION AND INSTRUMENTATION

Figure 1a is a LandSat Google Earth image of Manhattan, with pedestrian routes marked in yellow and fixed instrument locations marked with orange boxes. This RGB image portrays a sense of the variation in vegetation, building size and density, and albedo on the island. The axis of Manhattan is tilted at approximately 27° East of North, with *streets* running roughly East-West (with the street names of the various routes labelled in white) and *avenues* running roughly North-South, bounded by the Hudson river and the East river. There are approximately 16 streets per km if travelling along an avenue. Due to the inclination, at the time of the walks (between and 2 and 3 PM) the sun would be shining directly down the avenues, while pedestrians on the south side of the streets would be in shade.

Elevation also affects temperature, and **Fig. 1b** indicates the elevation in grayscale, with the main neighborhoods and Central Park marked. Elevations generally range from 1 to 2 meters above mean sea level (MSLE) near the rivers to up to 20 m in the center of the island, and up to 35 m MSLE in the Heights. The skyscrapers are concentrated in Downtown and Midtown where the bedrock is close to the surface, giving way to buildings of a few stories high in the

villages and Lower East Side (LES, which includes Chinatown) due to a much deeper soil layer. Central Park runs from 59th street to 110th street, with buildings becoming increasingly residential and lower in height while travelling northwards up the Upper West Side and Upper East Side (UWS and UES) into Harlem, with occasional government sponsored residential buildings that are 20 to 30 stories high but spaced apart in islands of greenery. Harlem and the Heights are mainly composed of tightly packed apartments of 4 to 7 stories high, row homes of 2 to 3 stories, and the occasional government project buildings described above.

Mobile Instrument Campaigns

The primary interest was to collect high resolution data rapidly, necessitating a temperature sensor with a fast response time. The Vernier Corporation surface temperature sensor is a plastic coated thermocouple at the end of a wire, and our tests found a response time on the order of 10 seconds, in agreement with the manufacturer's quoted values (see **Table 1**). This was matched with the Vernier RH sensor and Light Probe; all recorded on a Vernier Labquest 1 data logger.

Though these instruments are intended for educational rather than research purposes, the specifications for the temperature probe were close to the research grade instruments used in the mounted installations, and the combination of low heat capacity and continuous graphical readout made them ideal for field campaign purposes. Dewpoint was calculated from temperature and relative humidity via the Magnus formula (Aldukov & Eskridge, 1996).

Fig. 1 Mobile instrument pedestrian routes and fixed instrument locations (a, left). Elevations and neighborhoods (b, right).

The instruments were mounted on white cardboard, with the ends of the RH and temperature probes protected from sunlight by a Styrofoam cup (**Fig**. **2**). The thermocouple was positioned to be in free air in the middle of the cup. A light sensor was positioned looking roughly upwards, to be used not for quantitative analysis but to distinguish between direct sunlight and shadow during the walks. The instrument trays were affixed to backpacks filled with clothing to insulate the instruments from body heat, at a uniform 1.5 +/- 0.1 meters above the ground. The color and size of backpacks were not standardized. Based on our experiences we recommend that the instrument trays for future campaigns be improved by shielding the entire body of the RH meter from sunlight (the large horizontal cylinder shown in **Fig**. **2**) and aspirating the cup with a small fan.

Eight field workers were deployed at a time on either the street or the avenue routes shown in Fig. 1. Each walk started with several minutes for instrument acclimation after leaving public transport, then a simultaneous start at 2 pm, proceeding from West to East (streets) or North to South (avenues) for roughly 40 minutes - the time to walk across Manhattan. Field workers were instructed to walk at a constant pace from starting to stopping point, staying in shade when possible. Individual collection times were therefore dependent on walking speed, but measurements were detrended from regional temporal variations as described in the data processing section. Data was recorded every 10 seconds across the length of the route and binned into equal time segments during post processing. Typical walking speeds are between 1 and 2 m/s, yielding measurements every 10 to 20 meters That were averaged into larger segments.

Given the high buildings of Manhattan, GPS geolocation was not feasible. When data collection began in the summer of 2012, very few of the participants had smartphones capable of geolocation using cell tower triangulation, but by the summer of 2013 surveys could be made of walk timings and locations. As shown in **Fig**. **3** the normal dithering of cell phone geolocation results in a wandering path that only approximates the actual path taken, so we resorted to timing straight line segments and interpolating between these measured points. The interpolation was done by fractional time of the entire walk rather than absolute time: fast and slow walkers would spend the same percentage of the walk in each segment. Separation into segments also allowed correction to walking speed due to changes in elevation and street traffic. Crossings at intersections introduced a random element due to traffic, but these stops were found to be rarely more than 30 seconds, with an average stop every 3rd intersection of about 10 seconds due to the pedestrian tendency to cross as soon as traffic clears rather than wait for the cross signal. The random

element was more common on the avenue walks because of shorter blocks, though east-west traffic tends to be lighter and the stops shorter. The estimated variation due to traffic was ~30 meters, which influenced the bin size selected for post processing.
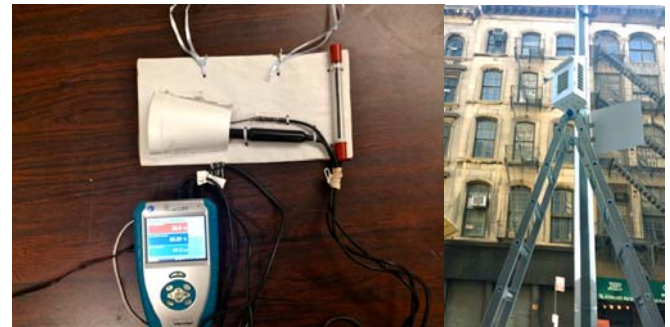

Fig. 2 Instrument mounts. Left: Vernier, mobile campaigns. Right: Hobo, fixed campaign
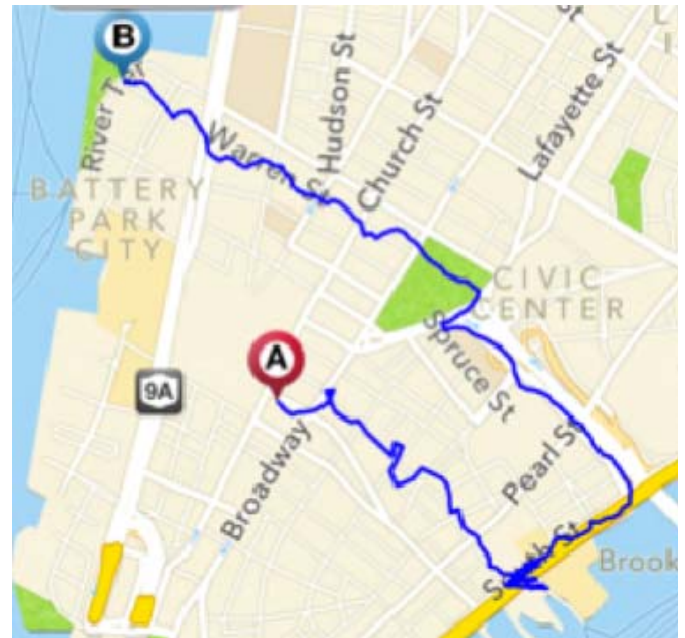

Fig. 3 Cell phone geo-location.

In 2012, eight street campaigns and two avenue campaigns were performed from late June through August, and nine street campaigns and eleven avenue campaigns were performed from mid-July through early October of 2013. Weather conditions were noted on each day. Route data from each day were inspected by eye and compared with others from the same day: those with obviously spurious data were rejected (missing data; more than 5 degrees or 10% RH difference). Bad data were attributed to bad batteries, operator error or insufficient wait time after exiting public transit.

Table 1 shows the accuracy, resolution, and response times of all instruments used. The slower response time of the mobile RH meter is primarily due to thermal inertia. So long as the mobile instruments do not pass near any sources of water vapor such as vegetation or large bodies of water, water vapor density should reflect

Table 1 Instrument specifications

Instruments	Resolution/ Accuracy	Response time
Vernier (*mobile*)		(still/moving air)
Temperature	0.03°C / 0.3°C	60 sec / 10 sec
Relative Humidity	0.04% / 10%	60 min / 40 sec
Hobo (*fixed*)		
Temperature	0.02°C/ 0.2°C	5 minutes : 1 m/s
Relative Humidity	0.1% / 2.5%	5 minutes : 1 m/s

the slowly changing air mass. In such cases we would physically expect the relative humidity to drop as the temperature increases (raising the saturation point), while dewpoint remains constant to reflect the unchanged water content of the air. In cases where the air temperature changes quickly as the walker passes into new surroundings, the temperature of the RH meter will lag the actual air temperature. So if the air temperature increases suddenly the RH meter will not register the expected drop in RH, reading higher than the true value, which would result in a higher calculated dewpoint. The reverse is true if temperature drops suddenly. In the case of rapid changes of temperature the effects of a temperature lag in the RH meter are therefore twofold. First, the physically expected anti-correlation between temperature and RH is muted by the lagged response. Second, the failure of RH to change produces a spurious positive correlation between temperature and dewpoint. This is seen in the raw data of **Fig**. **4a**.

The strong anti-correlation expected between temperature and relative humidity is not apparent in the raw data, while a strong correspondence is seen between the high frequency noise in the temperature and dewpoint. The correlations between temperature and (RH, DP) are (-0.52, 0.27). After averaging is applied

the high frequency responses are muted, and the correlations between T and (RH, DP) become (-0.75, -0.17). It should be noted that if temperature were not trending up while dewpoint was trending down, the correlation between DP and T in the raw data would have been more strongly positive, and in some datasets the correlations were as high as 0.85. For this particular instrument bias, averaging over a suitable time interval brings the numbers closer to physical reality for both RH and DP. The 2 minute average chosen for the mobile campaign is a balance between how quickly the physical surroundings are expected to change at typical walking speed, and the instrumental time lag.

Fixed Instrument Campaign

Ten Onset Corporation Hobo micro station data loggers were mounted inside white painted pine thermometer shelters (Ben Meadows, **Fig**. **2**), with a combination temperature and relative humidity probe suspended inside, and a solar pyranometer mounted outside facing upwards. The New York City Department of Transportation granted three months consent to mount the shelters on light posts from mid-June through mid-September. All were mounted from 3.1 to 3.7 m above the ground (depending on signage) on the south side of streets so that they would primarily be in shade (there were periods of direct sun in the mid-morning and late afternoon). They were set to collect data every three minutes in order to capture temporal variability due to convection. Where possible most stations were mounted directly above the street routes, with locations selected to capture the range of variability noted in the walking campaigns of 2012. As for the walking campaigns, dewpoint was calculated from T and RH.
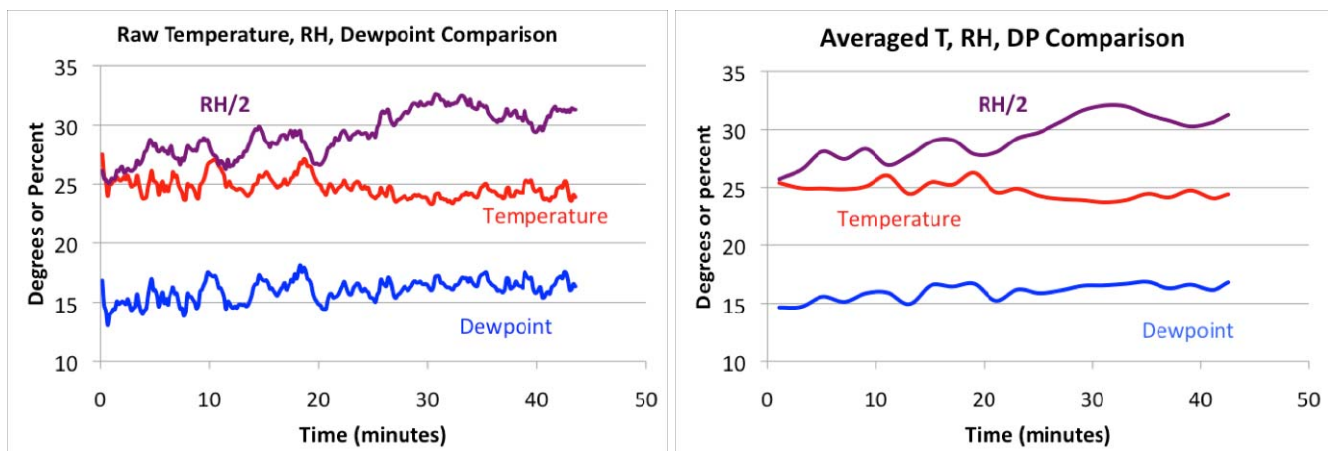

Fig. 4 The effect of RH lag time on relations between Temperature, RH, and Dewpoint. Note that RH has been divided in half to fit all variables on the same scale. (a) (Left) raw data. (b) (Right) data smoothed with a 2 minute average as used for the field campaigns.

Table 2 Instrument Deviations from the Mean

	Vernier T (C)	Hobo T (C)	Vernier RH %	Hobo RH %
Avg deviation from mean	0.2	0.04	1.3	0.5
Max deviation from mean	0.35	0.05	3.6	0.74
Max10 min variability	0.03	0.03	0.33	0.6
Avg 6 month drift	0.07	-	0.6	-
Max 6 month drift	0.15	-	1.2	-

Controlled Intercomparisons

Instruments were compared by placing the probes close together on a table in a large room, covered with a cardboard box to reduce convective and radiative gradients. After collecting data for 10 minutes the table was rotated 180 degrees and the process repeated. Comparison was done to the group average rather than to an absolute standard, which conforms to the data processing done for the field data. When both Vernier and Hobo instruments were on the table together, the averages for the two types of temperature measurements were within 0.05 C of each other, and the RH meter averages were within 2% of each other, with the Vernier showing the largest variation between instruments.

Based on the above procedure, measures of stability for the two types of instrument appear in table 2. The deviations from the average were used to correct each instrument readings towards the ensemble average. The variability shows the standard deviations of measurements during a 10 minute period. The drift of these deviations in the last row shows how much these corrections changed in a six month period. Note that the Hobo drift values were too small to be significant so are omitted.

DATA PROCESSING

Average anomalies were calculated for both campaigns, but the mobile campaigns required detrending so that all measurements on a day could be treated as though made at one time.

Mobile Campaigns

The purpose of the data set is to arrive at relative temperature and moisture differences between locations on Manhattan. To this end the walking campaign data set was processed in three steps:

1. Detrending data from temporal changes during the 40 minute measurement period

2. Binning detrended data from each route into line segments and averaging
3. Differencing each bin average from the Manhattan-wide average (forming anomalies) and normalizing by the standard deviation

Detrending is done by taking spatially fixed reference data (mean values from a set of station data in the NYC MetNet system, including Central Park), and performing a linear fit between the 2 pm and 3 pm reference data to arrive at reference values $V_{ref}(t)$ for each point in time during the measurement period ('V' stands for temperature, relative humidity, or dewpoint values). A measurement value V made at time t and position x will be converted into detrended data V_{dt} by

$$V_{dt}(x) = V(x,t) - V_{ref}(t) \qquad (data\ detrending) \qquad (1)$$

Note that this is based on a single reference trend rather than local trends, which could be expected to vary from location to location depending on radiative and evaporative effects. The result may be imperfect correction for temporal changes during the measurement period. The use of multiple stations averaged together for the reference trend reduces the chance that the detrending will be strongly affected by outlier stations.

Each route was divided into 20 equal segments by time (roughly 2 minutes or 12 measurements per segment) with averages taken over each segment. Fast walkers would thus have fewer points per segment, but cover the same geographical distance of roughly 150 meters (2 street crossings or about ½ a block from avenue to avenue). This distance corresponds to the surface temperature correlation length for urban settings found by satellite survey (Weng *et al.*, 2003).

After the data is detrended and averaged over route segments, Manhattan-wide averages and standard deviations are calculated. From these are derived the 'differences' and 'deviations' from the average at each location x, which are calculated as follows:

$$V_{diff}(x) = V_{dt}(x) - <V_{dt}> \qquad (\text{``differences''}) \qquad (2)$$

$$V_{dev}(x) = V_{diff}(x) / SD \qquad (\text{``deviations''}) \qquad (3)$$

The deviations represent how many standard deviations each measurement is from the average, which effectively normalizes the measurements each day to the unit Gaussian distribution centered on zero.

For each variable (temperature, relative humidity, dewpoint) the differences and deviations are averaged over all days for the street and avenue campaigns separately.
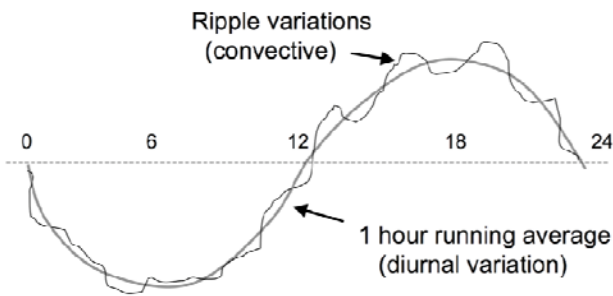
Fig. 5 Convective 'ripple variations' around diurnal variation. The differences between the ripple and diurnal cycle for each hour are used to calculate the temporal standard deviations.

Fixed Instrument Campaign

Beyond spatial anomalies, data reduction for the fixed instruments was focused on short term temporal variability (ripples in the data set), assumed to be due to primarily to convection. The convective cycle for cloud systems is roughly 30 minutes, so an hour (20 data points) is taken as the smoothing window to average out all variability on shorter time frames. Pairs of hourly data sets are formed from the raw data; hourly averages and hourly standard deviation of temporal variability. Averages are formed with an hour-long averaging window centered on each hour. The temporal variability is calculated in two steps: a 21 point running average is subtracted from the raw data to form a set of 'ripple differences' (**Fig**. **5**); then the hourly standard deviation is calculated from the set of differences in the one hour period bracketing each hour (30 minutes on either side of the hour mark).

Note that the hourly averages for the ten instruments can be used to calculate stable spatial anomalies free of temporal variation. This is the equivalent of applying **Eqs 2** and **3** as used for the mobile campaigns, but for hourly average data rather than detrended data.

RESULTS

Figure 6 (next page) shows average temperature and dewpoint anomalies for the street campaigns, represented as the mean number of standard deviations each location varies from the Manhattan average each day (referred to as "deviations" - see Data Collection and Instrumentation). On most days the Manhattan-wide temperature standard deviation was roughly 1 degree Centigrade. Dewpoint (DP) is shown rather than relative humidity (RH) because as a representation of the water vapor density, DP should be largely independent of temperature.

The statistical significance of the difference between the average of two data sets can be calculated using the Student T-test, which takes into account the standard deviations and sizes of both data sets. We wish to establish the statistical significance of the anomalies, differing from the average value of zero. These

anomalies at each location are composed of the measurements made at that location each day of the field campaign, converted into deviations. There is no single data set to compare these anomalies to, so an average data set is constructed with a mean value of zero, a standard deviation equal to the mean standard deviation of all the measured points on Manhattan, and a size slightly less than the total number of days in the field campaign (not all routes were measured each day, reducing the average number of measurements per location). The T values appear in **Figs 6b−6d**. To aid in interpretation, the approximate statistical significance of the T values appear in Table 3. For example if an anomaly in **Fig. 6a**, **b** has an associated T value of between 0.75 and 1.25 (red in **Fig. 6c**, **d**) the difference from the average is significant with confidence of 77% to 89%.

Figure 7 shows the equivalent of **Fig**. **5** for avenues. The measurements made along the avenues were generally in full sunlight, which is likely responsible for the patchwork pattern seen in **Figs 7 a, b** due to heating of the instruments. This is discussed in more detail in the interpretations section below, along with the method used to partially correct for differential heating by matching endpoints, marked with white bars. The result of endpoint balancing is shown in **Figs 7c−d**. This corrective procedure invalidates T-test calculations, which are therefore not shown.

The fixed instrument data can be treated the same way as the walking data: except done hourly instead of daily. Each instrument is averaged over an hour period to reduce noise, and then the average and standard deviation of the 10 instruments are calculated for that hour. Differences from the average are converted into deviations as in **Eqs 2** and **3**. **Figure 8** shows average anomalies of temperature and dewpoint for 2 am, 8 am, 2 pm, and 8 pm so that the afternoon measurement coincides with the starting time of the walking campaigns. The color scheme for deviations is the same as for **Figs 6** and **7**.

The deviations shown in **Fig. 8** represent spatial variability between locations, with the temporal variation averaged out. A comparison of the spatial and temporal variability for this set of instruments appears in **Fig. 9**. Spatial variability represents the differences between instruments, calculated as the standard deviation of the hourly averages of all 10 instruments. Temporal variability is the standard deviation of the ripple amplitudes indicated in **Fig. 5**, averaged over all instruments. The plots shown in **Fig. 9** are averages at each hour taken over the three month period the instruments were mounted in order to find the diurnal cycle of variability. This variability is crucial to interpretation of the deviation maps of **Figs 6-8**.

The average diurnal cycle of differences between the Hobo instruments can be calculated by multiplying the
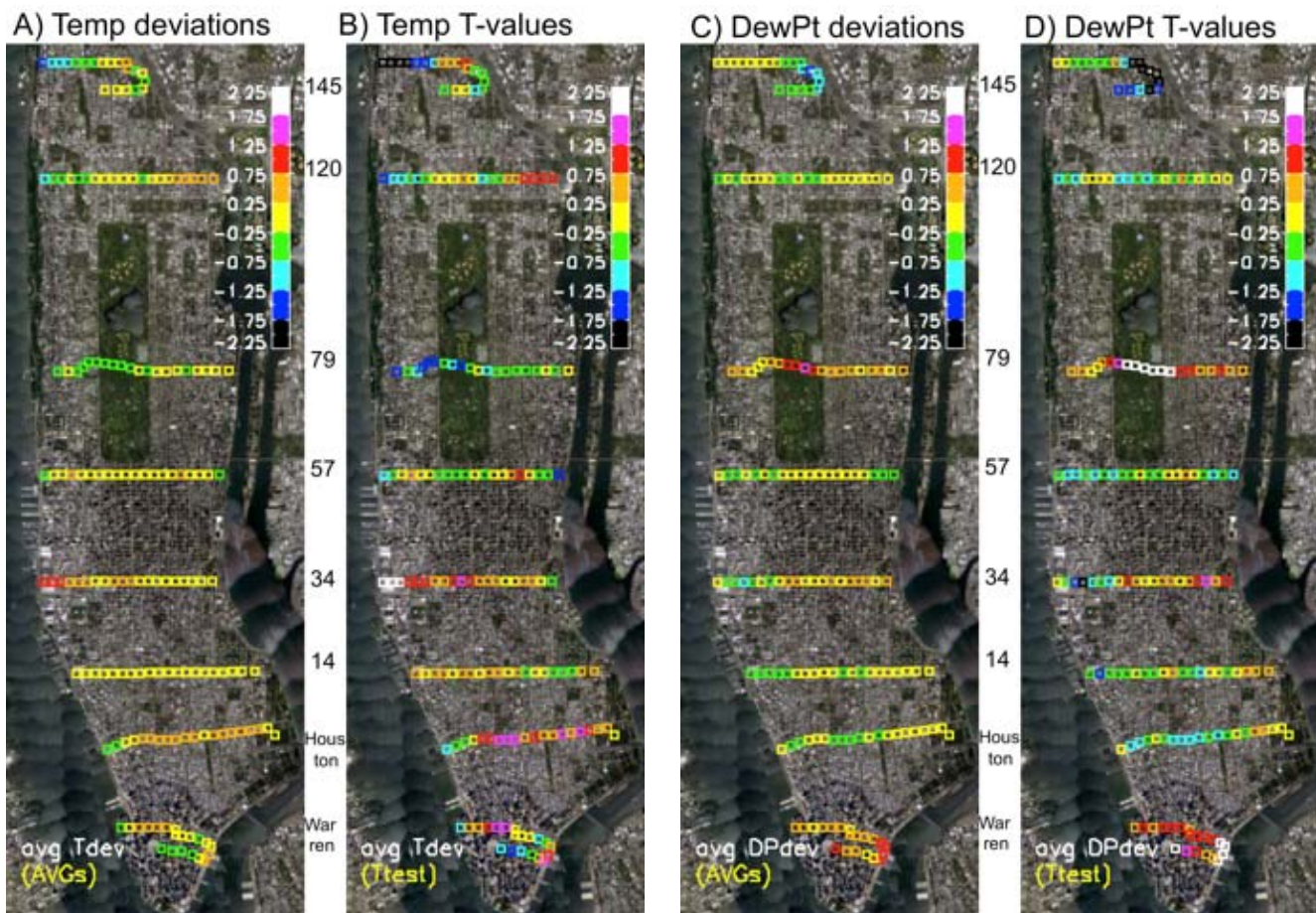
Fig 6 Street measurements of temperature and dewpoint anomalies. (A, C) Each colored square in A and C represents the mean number of standard deviations from which the measurement varies from the Manhattan average on the day each measurement was taken. (B, D) The Student T values in B and D are calculated using the mean and standard deviation of the measurements at that point compared to an "average sample" with a mean of 0, a standard deviation equal to the average standard deviation, and a number of points equal to the number of days measurements were done.

Table 3. T values and confidence levels for Fig 6 b,d

Symbol (positive) Colors (negative)					
T value	+/- 0.25	+/- 0.75	+/- 1.25	+/- 1.75	+/- 2.25
Confidence level	60%	77%	89%	97%	99%

spatial standard deviations in **Fig. 9** by the deviations in the maps of Figure 8. Interpreting the maps of **Figs 6** and **7** requires translation of the spatial and temporal deviations of the fixed instruments into those of the walking campaigns, and is discussed in the next section.

The datasets used to prepare all plots presented here are available for download on the website http://glasslab.engr.ccny.cuny.edu/u/brianvh/UHI.

PHYSICAL INTERPRETATIONS

General Trends

Some general trends are evident in the street data maps of **Fig. 6**. Temperature is lower in the Heights on the west ends of 145th and 120th streets, and higher in the low lying east sides of 120th and 14th streets. The

cooling effects of vegetation can be seen while traversing parks on 120th street and 79th street, and while near water on 57th, Houston, and Warren streets. Lower buildings allowing greater street insolation may also be responsible for warmer areas on 34th, Houston and 120th streets. The dewpoint generally increases near water and vegetation, and decreases with elevation. These observations have been paired with albedo, NDVI, building parameters and proximity to water, but a full statistical analysis of the correlations and cross correlations between these variables is beyond the scope of this paper. Preliminary results show that for the street data the strongest temperature correlation is to altitude, followed by vegetation (NDVI), building parameters and proximity to water.

The avenue data suffered a patchwork biasing effect between routes **(Fig. 7a, b)** almost certainly due to full insolation as compared to the shade of the street routes.
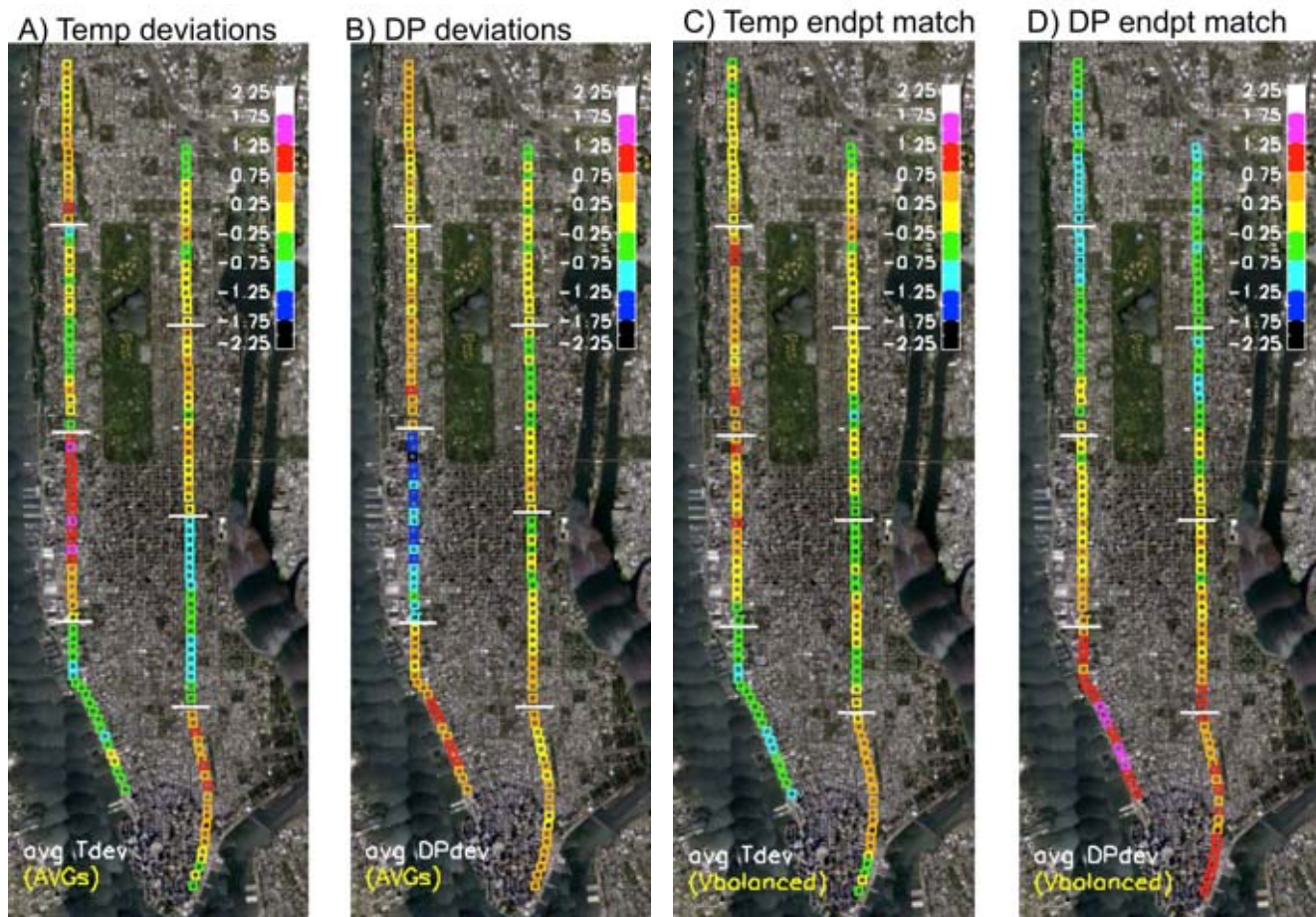
Fig 7 Temperature and dewpoint anomalies measured along avenues, with meanings for A and B as explained in figure 6. Boundaries between measurement routes are marked with white lines. The patchwork effect seen in A and B is likely due to solar heating of the relative humidity instrument, so endpoint matching is done in B, C. The procedure is described in the next section, but invalidates T-test calculations which are not shown.

The tendency was for dewpoint to drop as temperature increased. This is not due to the temperature lag between instruments; for if the temperature probe warmed more than the RH meter, the calculated dewpoints would be higher, not lower (this spurious correlation between temperature and dewpoint was discussed in the instrumentation section). The most likely explanation is that the RH meter is black and only the tip was shielded from solar insolation, so would warm more than the temperature probe, yielding lower RH and hence lower Dewpoints calculated based on the cooler temperature probe. The temperature probe was within a few cm of the RH meter inside an open Styrofoam cup, so likely would have been warmed, but less than the RH meter – explaining the opposite trends of temperature and dewpoint under insolation. Since the fieldworkers were consistently assigned to the same routes, individual route insolation biases may occur. All instrument packs were mounted at 1.5 meters; for short people this meant the instruments were near the tops of their backpacks, less likely to block the sun with backpacks or upper body. Tall people would have the instruments mounted halfway down their backs and were likely to be in shade.

These trends can be partially mitigated ('corrected' is too strong a term) based on two assumptions. The first is that the instruments are close to a steady state thermal balance, so that the correction for slow temporal trends based on the fixed MetNet instruments will apply to the mobile instruments despite insolation. The second assumption is that temperatures and dewpoints change slowly in space, so that adjacent measurements on the scale of the field campaigns are nearly the same. Though both assumptions violate the intended purpose of studying local differences in temperature and dewpoint, they allow us to address the patchwork pattern by requiring that the endpoints of adjacent routes be adjusted to the same values, and that this adjustment can be applied uniformly to the entire route. The West and East sides are independent, so after the individual route adjustments were applied both sides were adjusted uniformly to an average deviation of zero. All adjustments were constant across each route so that differences between adjacent points within each route were preserved.
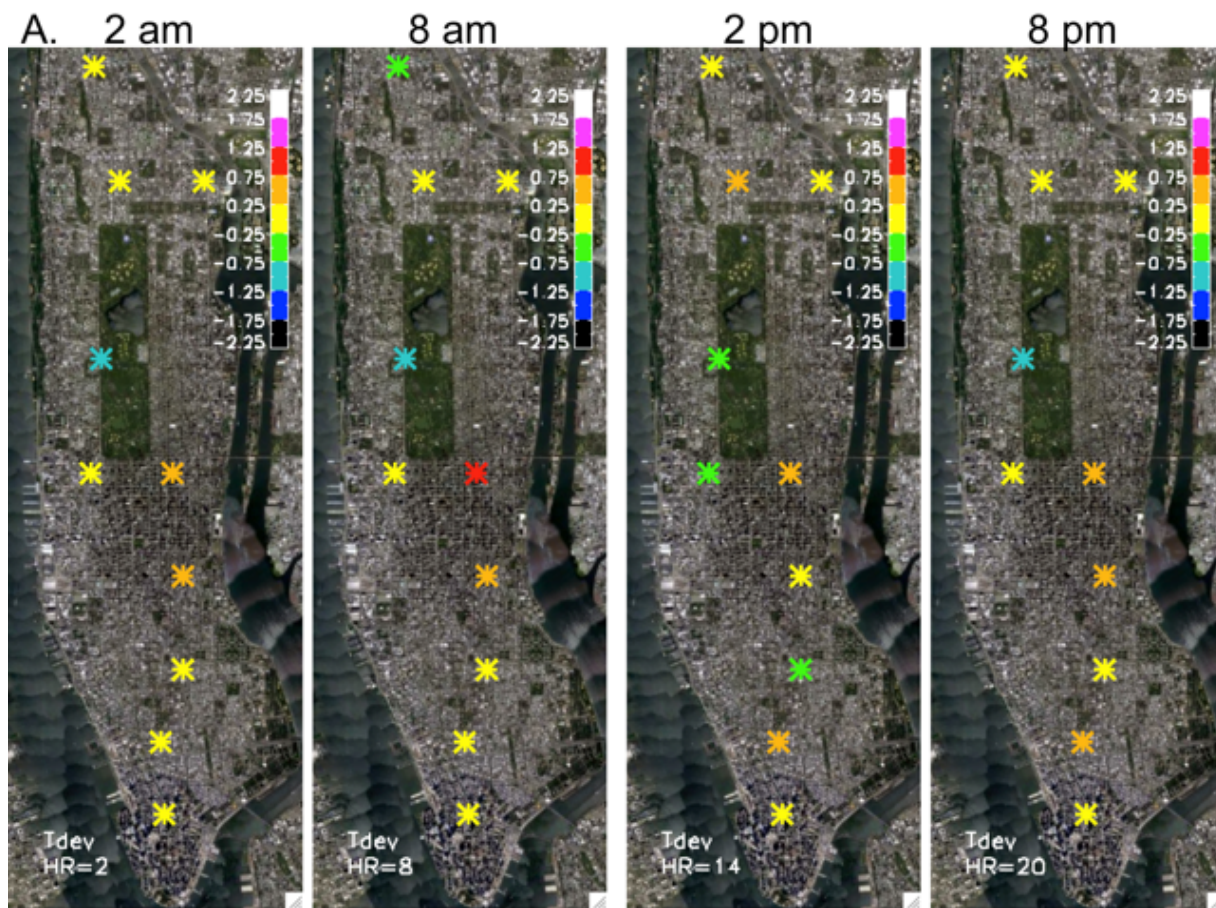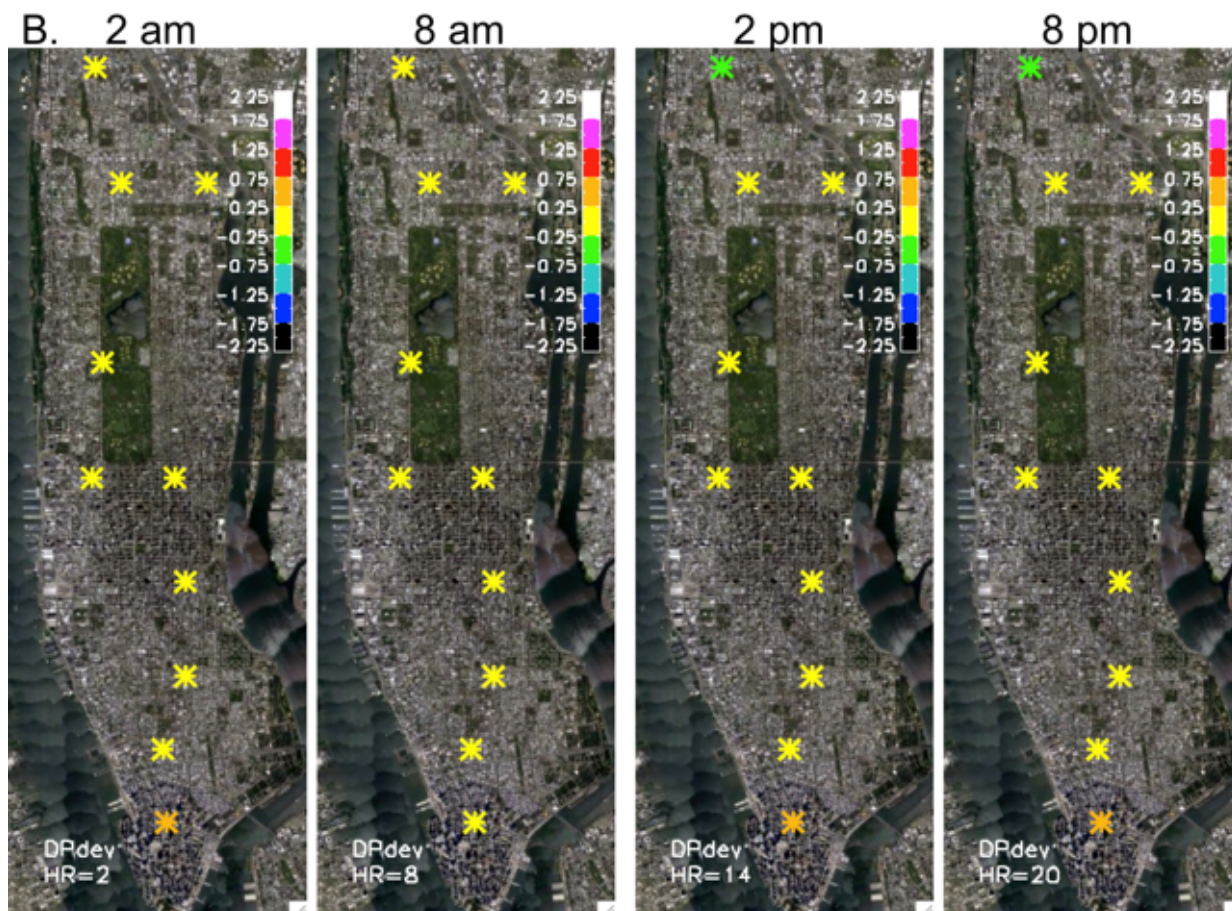
Fig. 8a Temperature Anomalies

Fig. 8 Fixed instrument average anomalies for selected hours of the day. (a) Temperature (top) (b) Dewpoint (bottom)
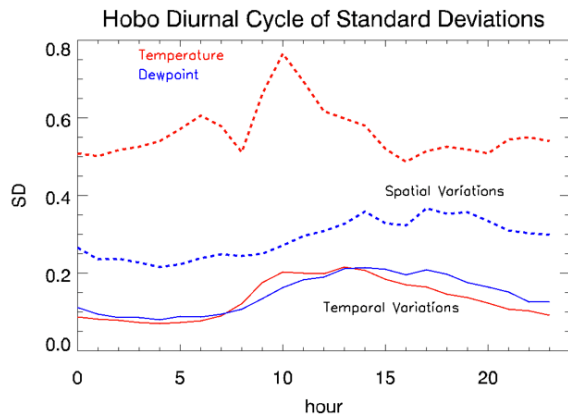
Fig. 9 Diurnal cycle of spatial and temporal variations for fixed Hobo instruments.

The results of the patchwork mitigation appear in **Fig. 7c, d**. In general the temperatures are lowest and dewpoints are highest near water, and with the exception of warm temperatures seen on the Upper West Side the trend of temperature and dewpoints dropping with elevation is also seen. The weakness of the patchwork mitigation scheme is most apparent in the warmer temperatures on the West versus the East sides in the upper 2/3 of Manhattan. For this reason this data is useful mainly for comparison within routes, and should only be trusted between routes where uniform values are seen for some distance on either side of the route junctions, as seen for temperature in the boundary between the bottom two routes on the West side, and the top three routes on the East side.

With these cautions in mind, preliminary statistical analysis shows that the temperatures in the insolated avenues correlate most strongly to albedo, closely followed by vegetation and building height. The effects of building height in avenues are opposite to the shaded street data: in the streets higher buildings have a cooling effect, while in the sunny avenues higher buildings have a warmer effect, likely due to increased reflection. Further numerical statements are being reserved for future publication.

The fixed instruments shown in **Fig. 8** show the largest temperature variation between locations in the morning, most likely because the sun shines down the streets before returning to shade (Note the 10 am peak in **Fig. 9**). The station mounted on 81 street along Central Park is cooler throughout the diurnal cycle, most likely due to transpiration and shade during the day, and not being in proximity to buildings which produce the signature night time urban heat island effect (Oke, 1982). In contrast, the dewpoint is far more stable, exhibiting slightly lower values in the northern heights and higher values at the southern tip, surrounded by water.

Comparison of Fixed to Mobile Measurements

The fixed Hobo stations were set primarily along street routes of the mobile campaigns. When comparing the maps of **Fig. 8** to **Fig. 6** it is important to recognize that the deviations are calculated from a much larger array of points for the mobile versus the fixed campaign. Given the geographical variability, it is not expected that the statistics of large and small samples will match, thereby shifting the deviations. Though absolute values may not be the same, relative differences between the same geographic points should have similar trends for the large (mobile) and small (fixed) data sets. Relative comparisons between the data sets exhibit a few points of obvious discrepancy: the east end of 120th street is warmer in the mobile campaign but cooler for the fixed instruments. Other points are less obvious when looking at a map: on 57th street to the east and west of Central Park the mobile data looks very similar, but the east appears much warmer in the fixed data set. This discrepancy is due to the standard deviations being much smaller among the fixed instruments (0.5 C on average versus 1.1 C on average in mobile instruments, which includes temporal variability), so that a small difference that would not cause a color change in the map of the mobile data set causes a change of two bins as seen in the fixed campaign map. With this in mind the similarity between the west side of 57th street and 81st street Central Park West in the fixed data must be marked as a discrepancy with the mobile data, which shows a cooler CPW at coarser resolution. Though the fixed and mobile routes are not co-located at 81st st CPW, the fixed instrument was shaded by trees while much of the mobile route at this point was exposed to sunlight, and should be warmer, not cooler.

A better understanding of these differences can be found by making comparisons day by day and location by location. This is done in **Fig. 10**, which compares the
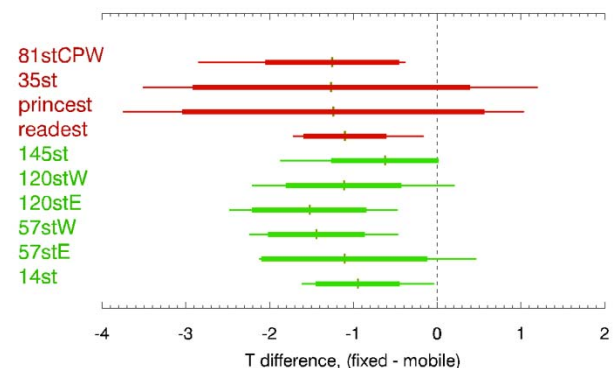

Fig. 10 Differences between mobile and fixed campaign measurements of temperature when mobile instruments pass by fixed locations. Green locations are co-located with mobile routes; red locations are generally 1 block north or south of the routes. Thick lines show 1 standard deviation on either side of the average (8 separate days), and thin lines show the maximum and minimum.

spread of temperature differences between mobile and fixed instruments. On each day temperatures are extracted from a two minute period of the mobile instrument that should correspond to closest proximity to the Hobo station. There were 8 days of mobile campaigns that overlapped with the fixed campaign, and for each location the temperature differences each day between the 2 minute average (12 measurements) of the mobile instruments were compared to the nearest fixed instrument (3 minute intervals). In **Fig. 10** the average difference for each site is enveloped by thick lines representing one standard deviation on either side of the average, and thin lines representing the minimum and maximum difference.

We see from this comparison that the fixed instrument temperatures are generally about 1 degree C cooler than the mobile temperatures, despite the fact that in carefully controlled intercomparisons they are identical. This is likely due to the difference in elevation: 1.5 m above ground versus 3.5 m for the fixed instruments. Such steep temperature gradients (5 times the adiabatic lapse rate - the theoretical limit for a stable atmosphere) are expected in the layer adjacent to solar heated surfaces, commonly seen in the afternoon (Cleugh and Grimmond, 2001). Though the shaded sides of streets where the measurements are made do not receive direct insolation, mixing within the streets would produce a similar temperature profile. The large variation in these differences at each location indicates the magnitude of local variability. The two largest variabilities between instruments occur in stations one block away from the mobile routes, shown in red.

The one degree difference between street level measurements and fixed station measurements is also seen in comparisons to the NYC MetNet data, which includes a collection of surface stations, many of them hobby stations mounted on rooftop. The diurnal cycle of variations between street level and fixed station data is of interest, and for this purpose a 24 hour campaign was built around a MetNet station on the Upper West Side near the Museum of Natural History. Six sets of measurements were made at fixed locations within two blocks of the station. For each measurement location the field worker would stand facing the sun (so the instruments on the back were in shadow), and collect data continuously for a 10 second average on either side of the street. Data was collected every two hours, a process of approximately 30 minutes. The winds were moderate, on the order of 3 to 5 m/s, with partially cloudy skies.

The results are shown in **Fig. 11**, with temperature and humidity used to calculate dewpoint. Station data for every 15 minutes is shown with a solid line, street measurements are crosses. The measurements began at 14:00 local time, with the hours wrapping around so that times above 24 hours are the next day. A warm front moved through at sundown (17:00 hours) on November

19, 2012, raising the dewpoint and holding nighttime temperatures steady until sunrise at hour 32 (8 am) the next morning. The street level data is generally a bit less than 1 degree warmer than the station data, with the greatest differences seen during rapid temperature changes, presumably due to the time it took to make the
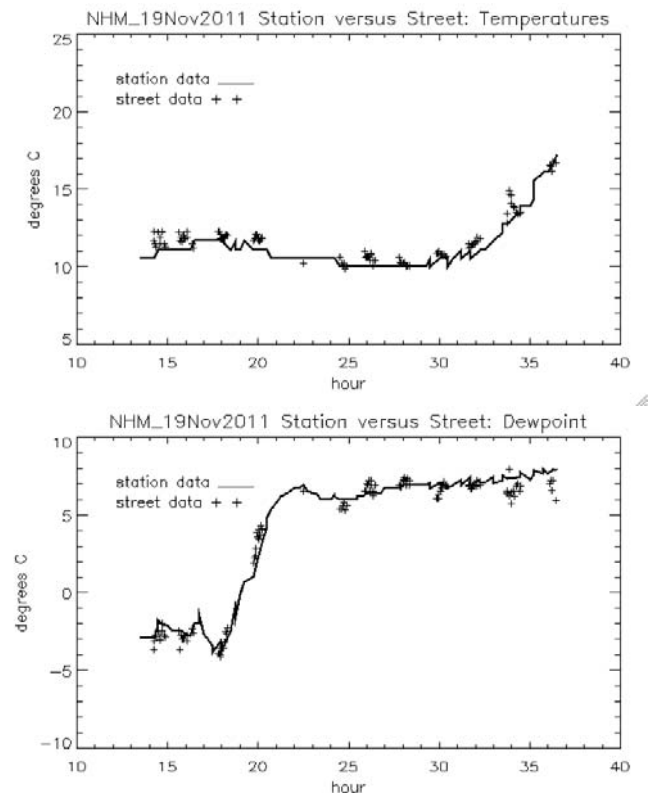

Fig. 11 Street level measurements of Temperature (a, top) and Dewpoint (b, bottom) compared to a station in the NYC MetNet system on Nov 19-20, 2011. Street measurements shown with crosses, station measurements by solid line. Data collected for 24 hours starting at 2 pm local time.

street level measurements. The dewpoints did not create such a consistent pattern between instruments, though at any given time the street measurements were nearly all either above or below the station data. The diurnal consistency of the cooler elevated station suggests that the nocturnal temperature inversion common in rural areas may not hold for urban environments due to heat storage and nocturnal emission (Oke, 1982).

Measures and Causes of Variability

In **Fig. 9** we see that the difference between fixed stations (spatial variability) is several times larger than the temporal variability seen at each station. The attribution of these temporal variations to convection is supported by a diurnal variation that matches solar heating. The sun also affects spatial variability in temperature, which peaks when the sun briefly shines directly down the streets around 10 am in the morning (the instruments are normally in shadow); a

corresponding afternoon peak is not seen perhaps because the air is well mixed by then.

The temperature differences between mobile and fixed instruments in **Figs 10** and **11** exhibit day to day variation that is related to that seen in **Fig. 9**. The nature of this variability is evident when comparing mobile measurements on two days with similar meteorology. **Fig. 12** shows temperature deviations on 57th and 34th street on June 8 and June 29, 2012. Both days had clear skies with WNW winds of about 3 m/s, and though June 29 was 8 degrees warmer we are only interested in the deviations from the average as shown. The most evident difference is the relative coolness of 57th street on June 29. We also see that the west end of 34th street is warmest on June 8, while the east end is warmest on June 29th. Since the surface environment has not changed (and there were no clouds), the only source of variation is the atmosphere. These moving hotspots most likely correspond to the convective structure of the atmosphere, and the distance between them of roughly 1 km corresponds to the typical scale of large convective eddies in the atmosphere that produce cumulus clouds.

The idea that convective variation is captured in the mobile measurements is supported by comparison between variability seen in the mobile and fixed instrument data sets. The mobile dataset for each day contains variability caused by spatial variations in the surface environment, and by temporal variations in the atmosphere. The standard deviation calculated from the mobile measurements each day can be related to the spatial and temporal variations captured in the fixed instruments by assuming a linear combination of the variances:

$$(SD_{mobile})^2 = \sigma \bullet (SD_{spatial})^2 + \tau \bullet (SD_{temporal})^2 \qquad (4)$$

The coefficients σ and τ are found by regression, which shows a correlation to spatial variability of 0.63 and to temporal variability of 0.35. **Fig. 13** shows that this vector combination of the two types of variability results in a better match to the mobile observations than either one alone. It should be noted that if the fixed Hobo instrument variability completely reflects the mobile instrument variability, the intercept must go to zero. This only happens when the two types of variability are combined.

With temporal correlations nearly twice as large as spatial correlations, it's reasonable to question whether local measurements are valid for wider regions. Before the field campaigns were launched, a test was made of the assumption that local measurements were representative of conditions within at least a block radius. Most of Manhattan is on a grid with parallel streets a uniform 80 meters apart. The Vernier
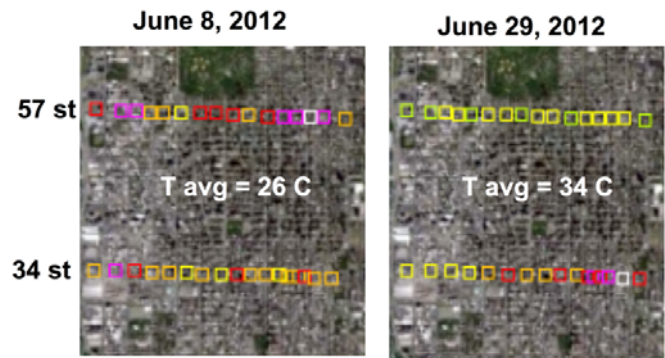

Fig. 12 Variable temperature anomalies on two days with similar meteorology. The color scale is the same as found in **Figs 6-8**.

instrument pack described above was deployed simultaneously on 146th and 147th streets, which are similar residential tree-lined streets that descend from a park on a cliff overlooking the Hudson, traversing a gentle hill of 10 m altitude above the starting and stopping points. The results are shown in **Fig. 14**, with a correlation between temperature datasets of 0.68 and correlation between RH datasets of 0.92. The rise in RH at the end may be due to an increase in tree cover on both streets. The sudden jumps in temperature in one dataset remain unaccounted for and may due to such things as proximity to pedestrians or other anthropogenic heat sources. Despite such irregularities, the correlations observed under the conditions of a one block separation were sufficient to justify a field campaign based on the techniques described in this paper.

DATA AVAILABILITY

The data sets described in this paper are available online at   http://glasslab.engr.ccny.cuny.edu/u/brianvh/UHI. The fixed Hobo instrument data sets are available in their entirety, plus hourly averages and hourly calculations of temporal variability. Due to the large amount of quality control and the confounding effects of convective variability, the mobile Vernier data set is only available as average anomalies calculated over the two summers. This set should reflect persistent spatial features due to surface characteristics, so a collection of surface feature data is available in two forms: co-located with the anomaly data, and as separate gridded data sets. The data has been regridded to square latitude-longitude grids, and are described in **Table 4**. The surface cover data sets will continue to evolve, with the MODIS vegetation and albedo data being replaced by LandSat, and the NBSD data set being replaced by New York City building level data. Up to date and more detailed descriptions of how the surface feature data sets are being created will be found on the website.
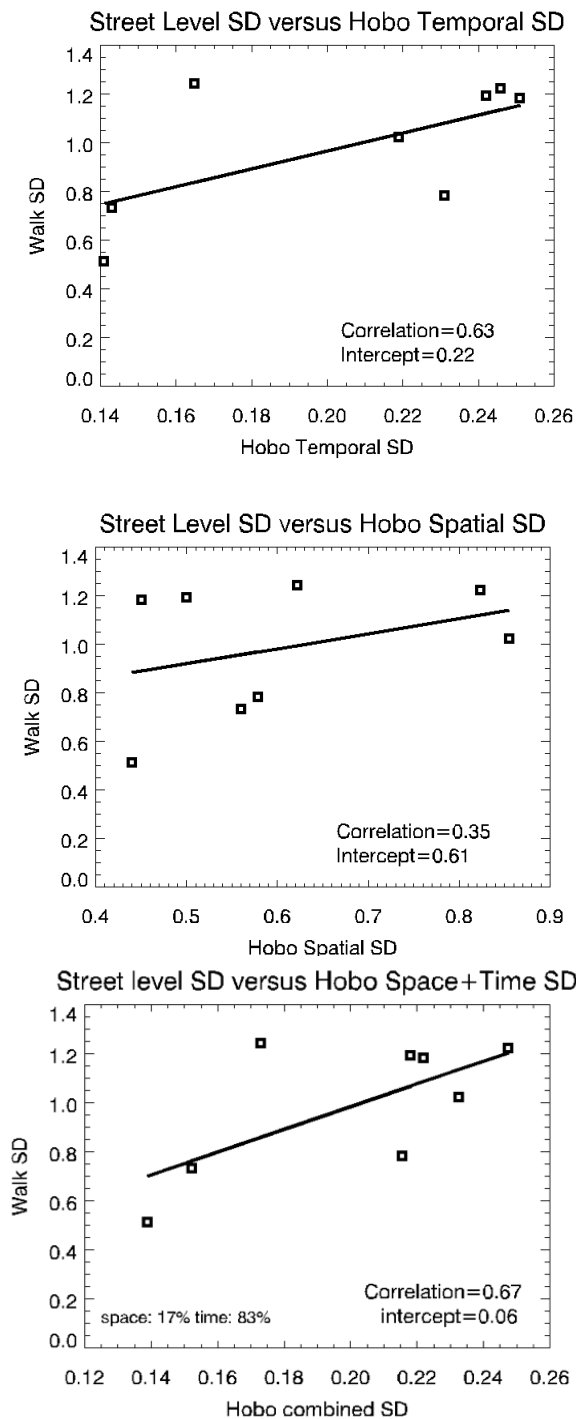
Street Level SD versus Hobo Temporal SD

Correlation=0.63
Intercept=0.22

Street Level SD versus Hobo Spatial SD

Correlation=0.35
Intercept=0.61

Street level SD versus Hobo Space+Time SD

space: 17% time: 83%
Correlation=0.67
intercept=0.06

Fig. 13 Variability in mobile temperature measurements versus spatial and temporal variability in fixed Hobo instrumentation for 8 different days. Standard Deviations of the mobile instrument measurements are plotted versus: (Top) Hobo spatial variations. (Middle) Hobo temporal variations. (Bottom) Vector combination of Hobo spatial and temporal variations.

To get a feeling for the content of the data sets, the RGB Google Earth images of **Figs 1** and **15** provides a visual estimate of albedo, and the elevation is shown beside it. The variation of surface cover is indicated in **Fig. 15**, in which vegetation (NDVI) is shown in green, building area fraction is shown in blue, and building height is shown in red; all at 0.025 degree resolution (approximately 250 m). The mixtures of colors show
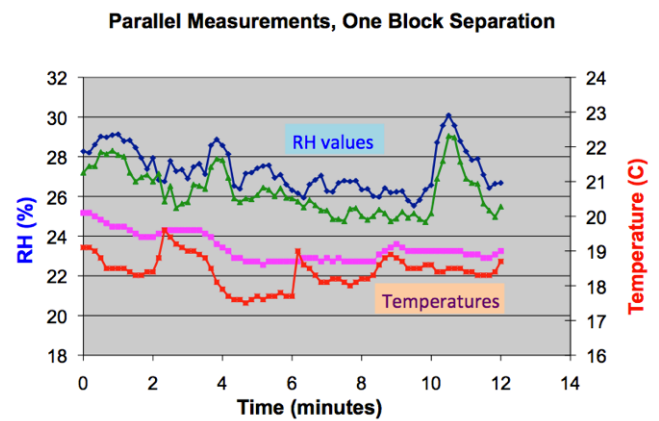

Parallel Measurements, One Block Separation

Fig. 14 Pedestrian measurements made one block apart, moving

in parallel variations in surface characteristics that will affect the persistent spatial anomalies of temperature. The coarse resolution seen in **Fig. 15** will degrade correlations between surface features and temperature-humidity measurements. For this reason a higher resolution LandSat data set is being prepared for albedo and NDVI, and with improved building data is expected to be posted to the website by summer of 2014.

CONCLUSIONS

The temperature and humidity dataset described in this paper is perhaps the highest resolution measurement of the street level structure of the urban heat island made to date. nineteen sets of mobile pedestrian measurements along Manhattan streets and thirteen along avenues over two summers were augmented by ten light-post mounted instruments recording every 3 minutes for 3 months.

Table 4. Current Surface Data sets

| Data Set	Resolution	Source	Description
Albedo	0.025 deg	MODIS satellite	Narrow to broadband conversion from visible and NIR
Vegetatn.	0.025 deg	MODIS satellite	NDVI: standard index calculated from red and NIR
Building Fraction	0.025 deg	National Building Statistics Database	Database of all major cities in USA, 250 m resolution
Building Height	0.025 deg	NBSD	See above
Elevation	0.005 deg	USGS	US geological survey
Water Proximity	0.005 deg	Based on USGS	Fraction of water within 1 km^2 centered on point. Water detected by elevations < 0.2 m above sea level.
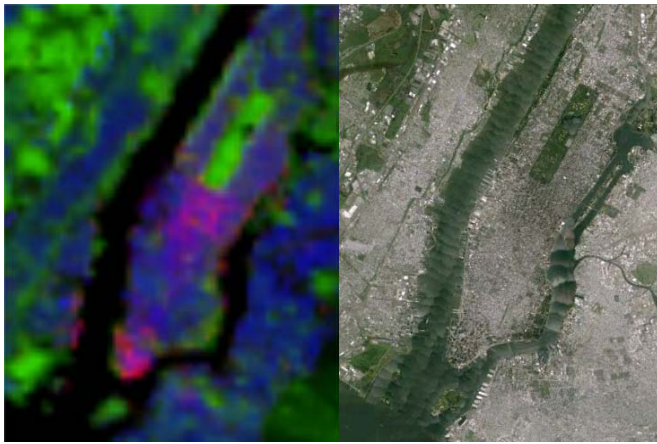
Fig 15 Composite of Building Height (Red), Building Area Fraction (Blue) and Vegetation index NDVI (Green) compared to a LandSat image of Manhattan. Low buildings with trees will thus appear blue-green; high buildings with vegetation will appear yellow.

The novel approach of scaling anomalies by the standard deviation of the day each measurement was made tends to weight the effects of all meteorological conditions equally rather than favoring the extremes. Variability in the daily mobile street level temperature measurements can be separated into persistent local anomalies induced by surface characteristics and moving patterns attributed to convection. The contributions of each to the total variability can be estimated from the high temporal resolution measurements of the set of fixed instruments, separated into spatial and temporal variability.

Statistical relationships between surface characteristics and temperature and humidity anomalies are under investigation, with the hope of being able to relate the size of the anomalies to present and predicted meteorological conditions. Such a model will be useful for predicting the fine structure of heat waves in the urban environment.

The mobile average spatial anomalies and fixed high temporal resolution data is available for download at the project website. The data is accompanied by surface characteristic data: estimated albedo, vegetation, building area fraction and height, and elevation. Descriptions of the ongoing progress of this project will also be posted on the project website.

REFERENCES

Alduchov, O. A., and R. E. Eskridge, (1996) Improved Magnus form approximation of saturation vapor pressure. *J. Appl. Meteor.*, **35,** 601–609.

Bottyán, Z. and J. Unger, (2003) A multiple linear statistical model for estimating the mean maximum urban heat island, *Theor. Appli.Clim.*, **75**, 233-243.

Burian, S., N. Augustus, I. Jeyachandran, M. Brown, (2008) *National Statistics Database Version 2.* Las Alamos Labs, document LA-UR-08-1921.

Cleugh, H. and C. Grimmond, (2001) Modelling Regional Scale Surface Energy Exchanges and CBL Growth in a Heterogeneous, Urban-rural Landscape. *Boundary-Layer Meteorology* **98**, 1–31.

Comrie, A. C., (2000) Mapping a wind-modified urban heat island in Tucson, Arizona (with comments on integrating research and undergraduate learning). *Bull. Amer. Meteor. Soc.*, **81**, 2417–2431.

Eliasson, Ingegard, (1996a) Intra-urban nocturnal temperature differences: a multivariate approach. *Climate Research* **7**, 21-30.

Eliasson, Ingegard. (1996b) Urban nocturnal temperatures, street geometry and land use, *Atmos. Environ.*, **30**, 379–392.

Fast, J.D., J. Torcolini, R. Redman, (2005) Pseudovertical Temperature Profiles and the Urban Heat Island Measured by a Temperature Datalogger Network in Phoenix, Arizona. *J. Appl. Meteo*, **44**, 3-13.

Gaffin, S.R., Rosenzweig, C., Khanbilvardi, R., Parshall, L., Mahani, S., Glickman, H., Goldberg, R., Blake, R., Slosberg, R.B. and Hillel, D., (2008) Variations in New York City's Urban Heat Island Strength Over Time and Space*, Journal of Theoretical and Applied Climatology,* **94**, 1–11.

Gedzelman, S. D., Austin, S., Cernak R., Stefano, N., Partridge, S., Quesenberry, S. and D. A. Robinson, (2003) Meoscale aspects of the urban heat island around New York City. *Theoretical Applied Climatology*, **75**(1-2), 29-42.

Grimmond, Sue *et al.*, (2010) Climate and more sustainable cities: Climate information for improved planning and Management of Cities (Producers/Capabilities Perspective*). Procedia Env. Sciences* **1**, 247-274.

Grimmond, Sue, (2007) Urbanization and global environmental change: local effects of urban warming. In *Cities and global environmental change*, Royal Geographic Society, London.

Grimmond, C.S.B, and T. Oke, (1999) Heat storage in urban areas: local-scale observations and evalutation of a simple model. *J. Appl. Meteor.* **38**, 922-940.

Haeger-Eugensson M, Holmer B. (1999) Advection caused by the urban heat island circulation as a regulating factor on the nocturnal urban heat island. *Int J Climatol* **19**, 975–988

Kinney, P., P. Sheffield, r. Ostfeld, J. Carr, R. Leichenko, P. Vancura, (2008a) Public Health. *New York State Energy Research and Development Agency (NYSERDA) Report 11-18: Response to Climage Change in New York State (ClimAID).* Chapter 11. http://www.nyserda.ny.gov/climaid

Kinney, P., M. O'Neill, M. Bell, J. Schwartz, (2008) Approaches for estimating effects of climate changes on heat related deaths: challengebs and opportunities. *Environmental Science and Policy.* **11**, 87-96.

Lu, D. and Q. Weng, (2006) Use of impervious surface in urban land-use classification, *Remote Sens. Environ.*, **102**(1-2), 146–160.

Meir, T., Orton, P., Pullen, J., Holt, T., Thompson, W., Arend, M., (2013) Forecasting the New York City urban heat island and sea breeze during extreme heat events. *Weather and Forecasting*, doi: http://dx.doi.org/10.1175/WAF-D-13-00012.1

Montavez JP, Rodrıguez A, Jimenez JI, (2000*) A study of the urban heat island of Granada. Int J Climatol* **20**, 899–911.

Oke, T.R., (1982) The energetic basis of the urban heat island, *Quart. J. Roy. Meteorol. Soc.*, **108,** 1–24.

Pena, Marco, (2009) Examination of the Land Surface Temperature Response for Santiago, Chile. *Photogrammetric Engineering & Remote Sensing*, **75**(10), 1191-1200.

Preston-whyte, R., (1970) A spatial model of an urban heat island. *Journal of applied meterology*. **9,** 571-73.

Rosenzweig C, Solecki W, Parshall L, Gaffin S, Lynn B, Goldberg R, Cox JS Hodges (2006) Mitigating New York City's heat Island with urban forestry, living roofs and light surfaces, in *Proceedings of the 86th Annual Meeting of the American Meteorological Society*, Jan 29–Feb 2, 2006, Atlanta, GA.

Steeneveld, G.J., S. Koopmans, B.G. heusinkveld, L.W. van Hove, A.A. Holtslag, (2011) Quantifying urban heat island effects and human confort for cities of vriable size and urban morphology in the Netherlands. *Journal of Geophysical Research* **116**, doi:10.1029/2011JD015988.

Stewart, Iain, Tim Oke (2009) Newly developed "Thermal Climate Zones" for defining and measuring urban heat island magnitude in the canopy layer. *Am. Met. Soc. Annual Meeting*, Phoenix, AZ. http://ams.confex.com/ams/pdfpapers/150476.pdf.

Weng, Qihao, D. Lu, and Jacquelyn Schubring, (2003) Estimation of land surface temperature-vegetation abundance relationship for urban heat island studies. *Remote Sensing of the Environment*, **89**, 467-483.

Weng, Qihao, H. Liu, B. Liang, D. Lu, (2008) The spatial variations of urban land surface temperatures: pertinent factors, zoning effect, and seasonal variability. *IEEE J. sel topics in appl. Earth obs rem sens.* **1**(2), 154-166.

Weng, Qihao, (2009) Thermal infrared sensing for urban climate and environmental studies: methods, applications and trends. IPRS J. Photgram. Rem. Sens. **64**, 335-344.

Yamashita, S. (1996) *Detailed structure of heat island phenomena from moving* observations from electric tram-cars in metropolitan area, *Atmos. Environ.*, **30**, 429–435.